A detailed Raman and X-ray study of UO_{2+x} oxides and related structure transitions

J. M. Elorrieta[1], L. J. Bonales[1], N. Rodríguez-Villagra[1], V. G. Baonza[2], J. Cobos[1]

[1]Centro de Investigaciones Energéticas, Medioambientales y Tecnológicas, CIEMAT Avenida Complutense, 40- 28040 – Madrid - Spain

[2]MALTA-Consolider Team. Departamento de Química Física I, Facultad de Ciencias Químicas, Universidad Complutense, 28040 – Madrid, Spain

CORRESPONDING AUTHOR

jonemiren.elorrieta@ciemat.es

Centro de Investigaciones Energéticas, Medioambientales y Tecnológicas, CIEMAT.

Departamento de Energía. Unidad de Residuos de Alta Actividad.

Av. Complutense, 40, 28040 Madrid, Spain

Telephone number: + 34 913460841

ABSTRACT

This work presents a detailed study of hyperstoichiometric UO_{2+x} ($0 < x < 0.25$) oxides and an assessment of the structural evolution taking place as oxidation proceeds. For this purpose, different UO_{2+x} powder samples, with controlled degree of non-stoichiometry, have been identified by thermogravimetrical analysis and characterized by X-ray diffraction (XRD) and Raman spectroscopy. XRD analysis reflects that the commonly assumed Vegard's law is not applicable over the whole hyperstoichiometry range, since a slight increase of the lattice constant is observed for $0.13 < x < 0.20$. A quantitative Raman analysis of the UO_{2+x} spectra as a function of the oxidation degree is also shown. A new method to characterize any UO_{2+x} sample (for $x < 0.20$), based on the shift of the 630 cm^{-1} band observed in the Raman spectrum, is proposed here for the first time. Moreover, three structure transitions have been detected at $x = 0.05$, 0.11 and 0.20, giving rise to four distinct regions associated with consecutive structural rearrangements over the hyperstoichiometry range: $x < 0.05$, $0.05 < x < 0.11$, $0.11 < x < 0.20$ and $0.20 < x < 0.25$.

KEYWORDS

Uranium dioxide, Hyperstoichiometry, Raman Spectroscopy, X-ray diffraction, Transitions.

1. INTRODUCTION

The oxidation of uranium dioxide (UO_2) has been widely studied due to the potential risks that this process may cause in the event of shielding failure during the storage of such a nuclear fuel.[1] In case of failure under dry interim storage conditions, the UO_2 matrix of the spent nuclear fuel (SNF) might be oxidized owing to its contact with the atmospheric oxygen and the high temperatures present due to the decay heat of the SNF.[2] The transformation of UO_2 into U_3O_8 via the two-step reaction[1] $UO_2 \rightarrow U_4O_9/U_3O_7 \rightarrow U_3O_8$ entails an increase in volume of around 36% and, consequently, it might cause the loss of integrity of the UO_2 matrix. Since this fuel matrix is responsible for retaining the fission products and transuranium elements formed by the irradiation process, release of radionuclides into the biosphere might occur.

UO_2 presents a fluorite-type crystal structure (Fm-3m space group, f.c.c.), where uranium U^{4+} ions occupy the octahedral sites and oxygen ions (O^{-2}) are located in the tetrahedral positions.[3] Owing to the presence of numerous empty interstitial sites, the UO_2 lattice is capable of accommodating additional oxygen ions. A slight lattice distortion in the cubic structure arises from the appearance of such point defects, thus leading to hyperstoichiometric UO_{2+x}.[4] As the amount of incorporated oxygen increases, the structure rearranges and extended defect-structures are formed. The most energetically favorable defect-structure proposed for around $UO_{2.12}$ is the 2:2:2 Willis cluster, which contains two anion vacancies, two <111> interstitial oxygens and two <110> interstitial oxygens, with no appreciable alteration of the uranium sublattice.[5,6] The limit phase preserving the fluorite structure is U_4O_9,[7] recently described as a superstructure of UO_2 consisting of "clusters of interstitial oxygen atoms embedded in a

distorted UO_2 lattice".[8] Further oxidation produces a change from the cubic to the tetragonal structure, corresponding to U_3O_7,[9] in which the cuboctahedral clusters are so close to each other (even sharing edges) that the cubic lattice suffers distortion and, subsequently, the *c/a* lattice parameters ratio is no longer equal to 1.[10] He and Shoesmith[6] studied the defect structures and phase transition in hyperstoichiometric UO_{2+x}, also including the tetragonal region of U_3O_7 ($0 < x < 0.33$ in UO_{2+x}), and identified four structural defect regions over the stoichiometry range: i) a random point defect structure ($x \leq 0.05$); ii) a non-stoichiometry region where point defects are gradually substituted by Willis 2:2:2 clusters ($0.05 \leq x \leq 0.15$); iii) a mixture of Willis and cuboctahedral clusters ($0.15 \leq x \leq 0.23$); and iv) cuboctahedral clusters ($x \geq 0.23$). Furthermore, it is well known that accommodation of a higher amount of oxygens within the U_3O_7 lattice results in a phase transition to orthorhombic U_3O_8.[9]

Traditionally, the techniques employed to analyze the reaction of UO_2 at atmospheric conditions have mainly consisted in thermogravimetry and X-ray diffraction (XRD). Thermogravimetric analyses reveal the kinetic behavior of UO_2 under these conditions, as well as the different mechanisms involved in each step of the process: diffusion governs the oxidation to U_4O_9/U_3O_7 (parabolic reaction kinetics) while the following step to U_3O_8 is controlled by a nucleation and growth mechanism (sigmoidal reaction kinetics).[1] Nevertheless, there are some uncertainties that have not yet been clarified, such as the real number of kinetic time domains and their detailed origin, as suggested by the studies carried out by Rousseau *et al.*[11] and Quémard *et al.*[12] On the other hand, XRD characterization has not only managed to determine the evolution of the already mentioned crystalline phases throughout the reaction[13] but, specifically, the change in the lattice constant of UO_2 during its transformation to U_4O_9/U_3O_7 (hyperstoichiometric

range).[7,14,15,16,17,18,19] A Vegard's law-like behavior over the whole hyperstoichiometric range has been proposed to explain such changes, but some scatter of the results is observed and discrepancies arise for the transition in the $0.125 < x < 0.17$ region.[15] This may be due to the complex oxide phase transformations that take place during the oxidation reaction.[11]

In recent years, an emerging technique like micro-Raman spectroscopy is gaining ground, since it meets two relevant features: it allows focusing on a particular area of the size of few micrometers, and provides a spectral fingerprint to differentiate between chemically similar compounds. Raman spectra of several uranium oxide phases, such as UO_2, U_4O_9, U_3O_7 and U_3O_8 have been previously published.[8,20,21,22,23] Likewise, some studies have achieved to identify a progressive variation of the UO_{2+x} Raman spectrum according to the degree of non-stoichiometry.[6,24,25] However, none of these studies has analyzed this variation both quantitatively and associating a specific stoichiometry (x in UO_{2+x}) to each spectrum.

In spite of the large number of studies that have been carried out on this matter, a more specific characterization of the different uranium oxides involved in the conversion of UO_2 into U_3O_8 needs to be done for a better understanding of the structural and chemical evolution of the system. On this basis, the present study is focused on the first oxidation stage, from UO_2 to U_4O_9, with the aim of characterizing the UO_{2+x} ($x < 0.25$) hyperstoichiometric oxides in detail. For this purpose, several UO_{2+x} oxides with x ranging from ~ 0 to ~ 0.25 have been prepared, their stoichiometries have been checked by thermogravimetric analysis and characterized by Raman spectroscopy and XRD. Our aim here is to shed some light on the structural evolution of the $UO_2 \rightarrow U_4O_9$ reaction,

based on the analysis of the measured lattice parameters and Raman shifts of a UO_{2+x} series of compounds.

2. EXPERIMENTAL

Sample preparation

U_3O_8 powder provided by ENUSA was reduced in an alumina furnace at 1000°C under a constant N_2:H_2 96:4 v/v gas flow to ensure that quasi-stoichiometric UO_2 powder was obtained. Afterwards, this powder was subjected to different times and temperatures in air atmosphere in order to attain homogeneous UO_{2+x} specimens with x ranging from 0 to $x \sim 0.25$. In this way, nine samples were prepared and their stoichiometry thereafter determined by thermogravimetric analysis.

Analytical equipment

Thermogravimetry experiments were carried out by means of a TA Instruments Q50 thermobalance under a synthetic air flow with a constant rate of 60 mL per minute. The samples were heated to 700°C in order to attain a complete conversion to U_3O_8. The weighing precision of the thermobalance was 0.01%. The O/U atomic ratios of the initial samples were then calculated by assuming that oxidation to U_3O_8 was fully completed. U_3O_8 complexion was afterwards verified by XRD (data not shown).

Raman spectroscopy analyses were performed with a Horiba LabRam HR evolution spectrometer with 800 mm focal length. All spectra were acquired at an excitation wavelength of 632.8 nm provided by a He-Ne laser. The laser beam was focused on the sample through the 100x objective of an Olympus BX41 microscope. The excitation

power was optimized and minimized to avoid alteration of the samples. The scattered radiation was then collected in backscattering geometry, dispersed using a 600 grooves/mm holographic grating and recorded using a CCD detector (256 x 1024 pixel), obtaining a ~1 cm^{-1}/ pixel resolution and an spectral resolution better than 3 cm^{-1}.

For the analysis of each sample, an average of 20 spectra recorded at different locations of the sample were acquired over the wavenumber range from 250 to 1300 cm^{-1}.

XRD characterization was performed by means of a Philips PANalytical X'Pert MPD diffractometer using Cu K_{α_1} radiation (λ=1.54056 Å) and operating at 45 kV and 40 mA. A Bragg-Brentano configuration geometry was used. The 2θ range covered was from 20° to 120°, at 0.04° scanning steps. Four to six XRD patterns were acquired under identical conditions for each sample. The uncertainty of each XRD measurement was estimated as the standard deviation of the individual measurements.

Both Raman and XRD experiments were performed in air under STP conditions.

3. RESULTS AND DISCUSSION

Thermogravimetric analysis

Fig. 1 shows the thermogravimetric curves obtained for selected samples, which reflect the typical two-step oxidation of UO_2 ($UO_2 \rightarrow U_4O_9/U_3O_7 \rightarrow U_3O_8$).[1] All the samples present a similar general behavior when heating them to 700ºC: a weight gain is first observed when a temperature of 200-250ºC is reached; at that point, the samples begin to oxidize (weight gain increase) until a plateau appears at around 300-400ºC,

associated with U_4O_9/U_3O_7;[26] finally, oxidation continues and at 450-500ºC another plateau is reached, indicating that conversion to U_3O_8 has been fully completed.[26]

The stoichiometry of the different samples was calculated from the weight-gain data recorded in the thermogravimetric analyses, thus determining their correspondence to the hyper-stoichiometric oxides $UO_{2.03}$, $UO_{2.05}$, $UO_{2.07}$, $UO_{2.09}$, $UO_{2.11}$, $UO_{2.15}$, $UO_{2.17}$, $UO_{2.20}$ and $UO_{2.24}$, with a relative sampling error around 1%.

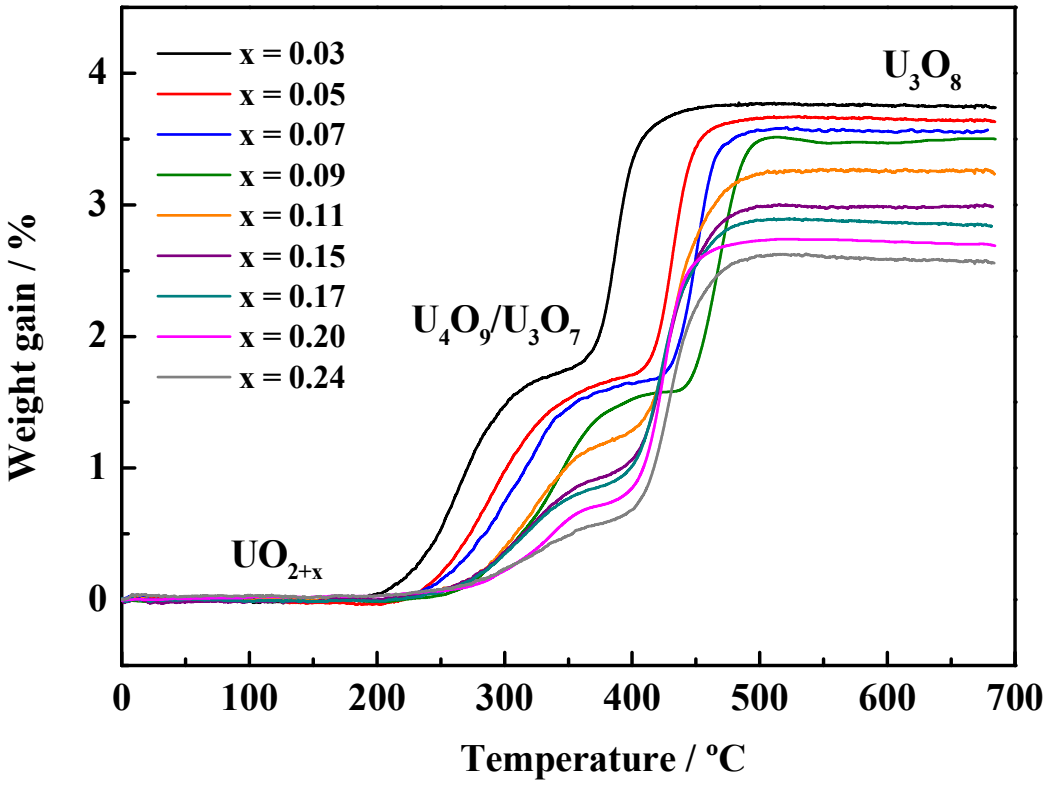

Fig. 1. Thermogravimetric curves of the UO_{2+x} hyper-stoichiometric oxides.

It should be noted in Fig. 1 that each hyperstoichiometric oxide starts oxidizing at a different temperature, which is lower as the initial degree of non-stoichiometry

increases. Likewise, the first (short) plateau reached, related to U_4O_9/U_3O_7,[26] is narrower for more oxidized samples. It can also be appreciated that the oxidation rate (slope) in both steps ($UO_{2+x} \rightarrow U_4O_9/U_3O_7$ and $U_4O_9/U_3O_7 \rightarrow U_3O_8$) significantly varies for the different hyperstoichiometric oxides, especially in the initial transformation to U_4O_9/U_3O_7.

XRD analysis

Typically three X-ray diffractograms were acquired for each sample. As an example, we show in Fig. 2 selected reflections of the different oxides patterns: (111), (200), (220) and (311). For the sake of comparison, we reproduce (open symbols) the diffraction pattern of the cubic structure of stoichiometric UO_2 reported by Fritsche (ICDD 00-041-1422).[27]

A general upshift in 2θ of all the peaks can be appreciated as the degree of non-stoichiometry increases, being particularly remarkable for the (111) reflection (see dotted line in Fig. 2). It is also noteworthy that both (200) and (311) reflections show satellite peaks at higher angles (asterisks in Fig. 2) from $UO_{2.11}$ on, their contributions becoming more relevant with increasing *x*. This has been attributed both to the U_3O_7 tetragonal phase and to the U_4O_9 cubic superlattice,[28,29,30,31] and their observation must be related to the formation of cuboctahedral oxygen clusters, as postulated by Nowicki *et al.*[32], because U_4O_9 and U_3O_7 polytypes only differ in the spatial arrangement of such clusters and the subsequent lattice distortion.

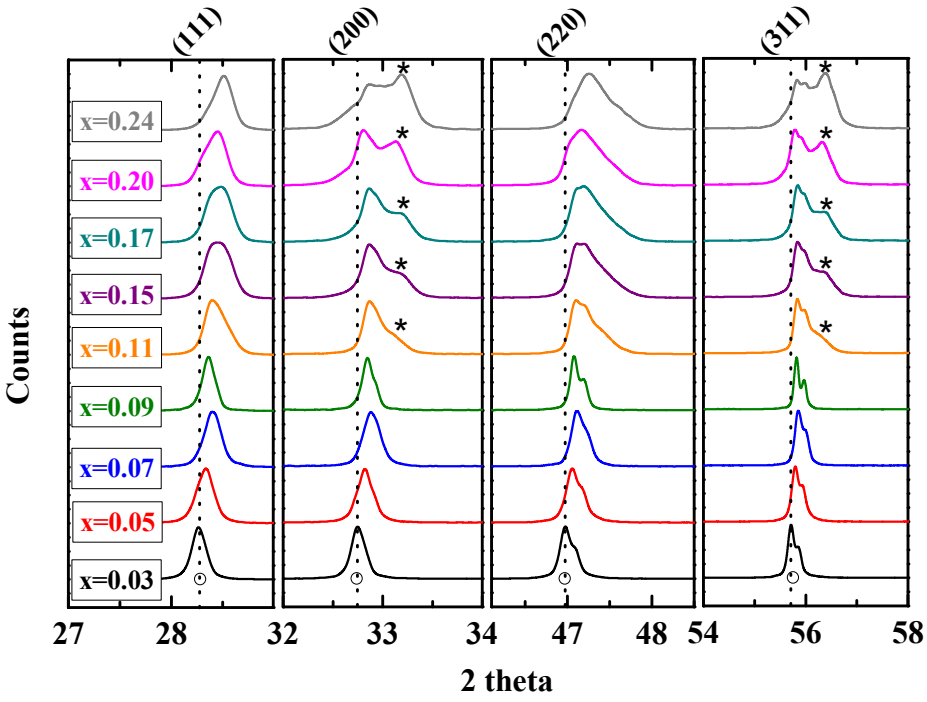

Fig. 2. Comparison of the (111), (200), (220) and (311) XRD reflections of the hyperstoichiometric oxides studied in this work. Asterisks indicate the appearance of a new diffraction peak. Open symbols correspond to the ICDD 00-041-1422 UO_2 pattern.[27]

In order to quantify the evolution of the structure with x, the lattice constant (a_0) of every UO_{2+x} oxide was calculated from the results shown in Fig. 2 applying Bragg's law and assuming that the system remains cubic throughout the whole hyperstoichiometric range;[7] the analysis is shown in Fig. 3, showing rather good agreement with data from other authors measured under similar conditions.[14,15,16,17,18] Differences observed with the results of Lynds *et al.* [15] in the $0.7 < x < 0.12$ range might be due to the elevated-temperature quenching treatment performed by these authors during sample preparation.

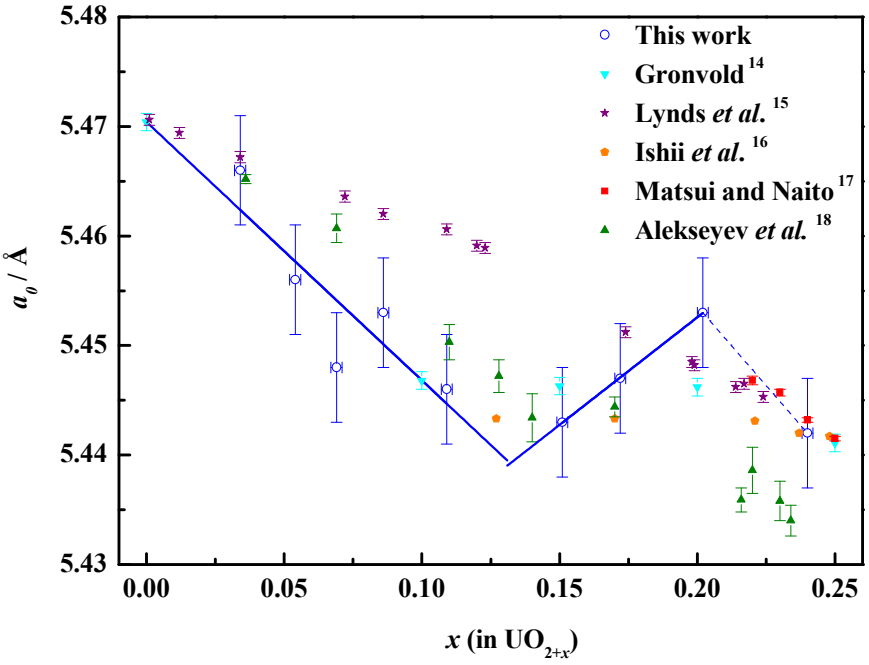

Fig. 3. Lattice constant as a function of x for the different UO_{2+x} oxides. Open symbols represent experimental data obtained in this work, whereas solid symbols illustrate data published by other authors indicated in the legend. Straight lines correspond to linear fits (see text for details).

The variation of the UO_{2+x} lattice constant is assumed to follow Vegard's law in the hyperstoichiometric range ($0 < x < 0.25$),[7,14,15,16,17,18], which implies a linear decrease on the lattice constant with an increase in the degree of non-stoichiometry. This law seems to hold in the $0 < x < 0.13$ range, but a change in the slope is observed around $x = 0.15$ to again decrease in the $0.17\text{-}0.22 < x < 0.25$ region, which is commonly associated with U_4O_{9-y}.[15,16,17,33]

Vegard's law in the $0 < x < 0.13$ range yields Equation 1, which has been obtained from a linear fit to our experimental data.

$$a_0\,(\text{Å}) = 5.470 \pm 0.006 - (0.24 \pm 0.08)\,x, \quad (0 < x < 0.13) \qquad \text{(Eq. 1)}$$

The intercept in Equation 1, *i.e.* the lattice constant for stoichiometric UO_2 (5.470 Å), is in good agreement with the values estimated by other authors.[14,15,18,34] Nevertheless,

larger discrepancies are observed with the slopes reported by Lynds *et al.*[15] (-0.094) and Alekseyev *et al.*[18] (-0.1495), very likely due to the different preparation and measurement conditions employed by these authors.

In spite of the consensus observed for $x < 0.13$, some uncertainty was reported by Lynds *et al.* [15] concerning the variation of the lattice constant in the intermediate region $0.13 < x < 0.17$. These authors obtained scattered results of the lattice constant in this region and were unable to obtain a unique Vegard equation across the whole hyperstoichiometric range; instead, they split it into two different equations below $x = 0.13$ and above $x = 0.17$. They attributed this observation to a transition detected at $x = 0.125$ by some authors when analyzing the partial molar free energy of oxygen in UO_{2+x}.[35] Moreover, scarce values concerning this intermediate region have been reported.[14,16,18] However, our results clearly demonstrate an increase of the lattice constant in the region $0.13 < x < 0.20$, which can be described by Eq. 2.

$$a_0\,(\text{Å}) = 5.4133 \pm 0.0005 + (0.196 \pm 0.003)\,x, \quad (0.13 < x < 0.20) \qquad \text{(Eq. 2)}$$

Previously published lattice constant values within $0.13 < x < 0.20$ are indeed in accordance with the trend observed here; however, to the best of our knowledge, this is the first time that a non-Vegard behavior is reported for this particular region. This obviously confirms that a single linear equation is not sufficient to calculate x over the whole UO_{2+x} range.

Concerning the lattice constant in the $0.20 < x < 0.25$ region, *i.e.* the U_4O_{9-y} range, it seems to follow a Vegard's law-like behavior (dashed line in Fig. 3) in accordance with results published by different authors.[15,16,17,33] Nevertheless, additional data are required in order to verify such tendency and to establish an equation over the entire U_4O_{9-y}

region; ongoing work is being carried out in our laboratory on this subject. In any case, the important conclusion that can be derived from the results of Fig. 3 is that it is impossible to give a reliable value of the oxidation degree (x) of a given UO_{2+x} oxide in the $0.05 < x < 0.25$ range only with the help of an X-ray pattern. So we need complementary techniques in order to properly characterize hyperstoichiometric oxides.

The above XRD results however help to identify two structural transitions at $x = 0.11$ and $x = 0.20$. As the oxidation degree increases, the lines of the XRD patterns fairly correspond to those of UO_2 (see Fig. 2), except for their steady displacement to higher angles commonly associated with non-stoichiometry in UO_{2+x}.[13] Then, a change is appreciated starting around $x = 0.11$ with the appearance of a new peak next to some reflections (labeled with asterisks in Fig. 2) which was already attributed to the formation of cuboctahedral oxygen clusters. This clearly might correspond to the transition observed at $x = 0.125$ by some authors,[35] and agrees with the kink in the variation of the lattice constant around $x = 0.13$. A second transition is observed at around $x = 0.20$, attributed to U_4O_{9-y}, as revealed by the trend of the lattice constant, and the Vegard's law is recovered indicating that a lattice contraction is again taking place.

Raman spectra analysis

Several Raman spectra recorded at different points of every sample were analyzed and compared. All spectra acquired for each particular oxide were very similar, thus confirming the homogeneity of the samples. Each spectrum plotted in Fig. 4 corresponds to the average of at least 20 individual spectra to improve the signal-to-noise ratio.

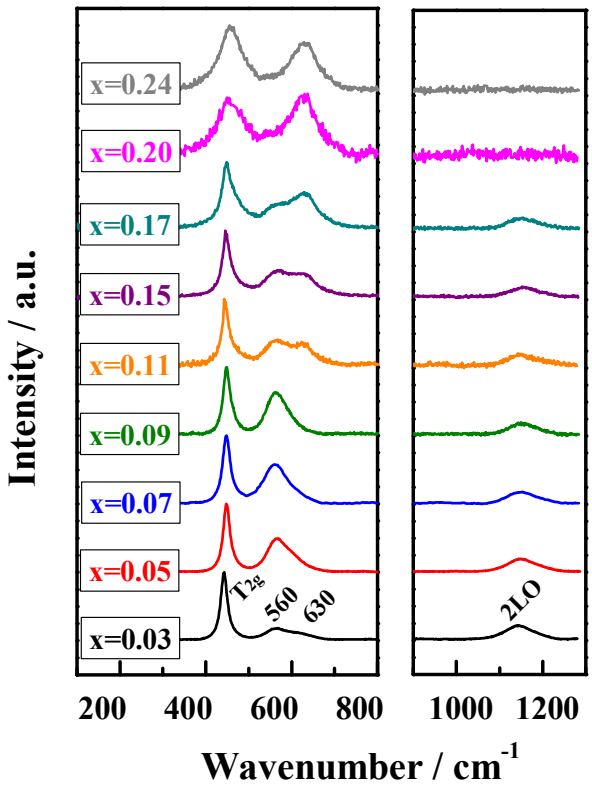

Fig. 4. Raman spectra of the UO_{2+x} hyper-stoichiometric oxides.

Since the space group corresponding to the fluorite-type structure of uranium dioxide is Fm-3m (O_h),[36] group theory predicts two vibrational modes for UO_2: a triply degenerate Raman active mode (T_{2g}) and an infrared active mode (T_{1u}). The Raman spectrum of a stoichiometric UO_2 shows two bands located at 445 cm^{-1} and 1150 cm^{-1}, respectively.[36] The band observed around 445 cm^{-1} can therefore be attributed to the T_{2g} vibrational mode,[37] while the band observed around 1150 cm^{-1} has been assigned by Livneh and Sterer[38] to a second order longitudinal optic phonon (2LO), despite the fact that it was previously assigned to a crystal field electronic transition.[39]

The initial hyperstoichiometric $UO_{2.03}$ spectrum contains the same Raman bands as stoichiometric UO_2 and an additional broad and asymmetric feature (500-700 cm^{-1}) which can be considered the result of two main contributions centered around 560 and 630 cm^{-1}. The first can be associated with the 555 cm^{-1} broad band observed by Guimbretière *et al.*[40] at the grain boundary of non-irradiated UO_2 and the one around 550 cm^{-1} found by Livneh and Sterer[38] when characterizing UO_2 at low excitation energies. The band observed around 630 cm^{-1} has been attributed to anion sublattice distortions,[11] which in our case would be caused by the excess of oxygen. However, this band has been also specifically associated to a structural defect of cuboctahedral (U_4O_9) symmetry.[8]

The evolution of the Raman spectrum at different degrees of oxidation is shown in Fig. 4. The changes observed can be summarized as follows: 1) a continuous broadening and upshifting of the 445 cm^{-1} band, 2) a significant decrease in intensity of the 2LO band, which essentially disappears at a certain point between $UO_{2.17}$ and $UO_{2.20}$, 3) a continuous increase in the intensity of the ~630 cm^{-1} band as the oxygen content increases, and 4) changes in the relative intensity of the ~560 cm^{-1} band, showing a maximum around $x = 0.09$.

A detailed band-profile analysis of the spectra was carried out to track the evolution of the characteristic wavenumbers, including those bands contributing to the broad feature observed in the 500-700 cm^{-1} spectral range. A second derivative analysis allowed us to obtain the wavenumber of four main contributions, namely, the T_{2g} band at around 445 cm^{-1}, two overlapping bands at ~560 and ~630 cm^{-1} and the 2LO band at ~1150 cm^{-1}. Then a multiple Lorentzian fit was conducted, using the obtained wavenumber values as fixed parameters. An example of this profile analysis is given in Fig. 5 for $UO_{2.03}$ and

$UO_{2.24}$ in the 300-800 cm^{-1} range. The following changes were found between the wavenumbers of the main Raman bands in both compounds: the 445 cm^{-1} band is shifted to 459 cm^{-1} for $UO_{2.24}$ and the bands observed at 562 and 623 cm^{-1} in $UO_{2.03}$ are centered at 547 and 637 cm^{-1} in $UO_{2.24}$.

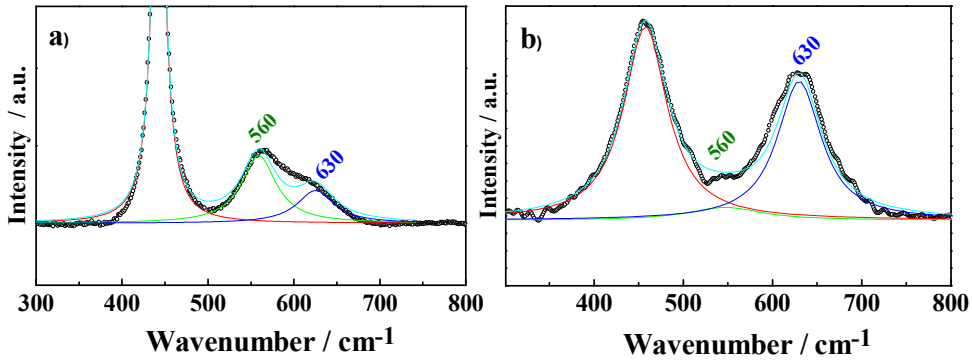

Fig. 5. Profile analysis of a) $UO_{2.03}$ and b) $UO_{2.24}$, illustrative of the two bands detected in the 500-700 cm^{-1} range for all UO_{2+x} oxides: the ~560 and ~630 cm^{-1} bands.

A quantitative analysis of the evolution of the Raman spectra with x similar to that performed above with our XRD results can be performed on the basis of the 445 cm^{-1} (T_{2g}) band shift, which provides information about the overall fluorite lattice, and the intensity and shift of the 630 cm^{-1} band, which can be associated with a distorted oxygen sublattice. As can be seen in Fig. 6a, the 445 cm^{-1} band first upshifts from $UO_{2.03}$ to $UO_{2.05}$, and then remains almost constant in frequency until $UO_{2.11}$ is reached. At this point, the band begins to substantially move towards higher wavenumbers, reaching the value of 459 cm^{-1} for $UO_{2.24}$. Fig. 6b shows the intensity of the 630 cm^{-1} band normalized with respect to the intensity of the 445 cm^{-1} band, *i.e.* I_{630}/I_{445}, as a function of x. As can be observed, the band at 630 cm^{-1} continuously increases in intensity as oxygen content increases. Concerning the wavenumber variation as a function of x, shown in Fig. 6c, an initial downshift is appreciated until $UO_{2.09}$; at that point, it

drastically shifts to a much higher wavenumber and continues downshifting from $UO_{2.11}$ to $UO_{2.20}$. Data corresponding to $UO_{2.24}$ do not follow the tendency of the latter oxides, what must be due to the fact that it belongs to the U_4O_{9-y} region, as indicated by the XRD results described above.

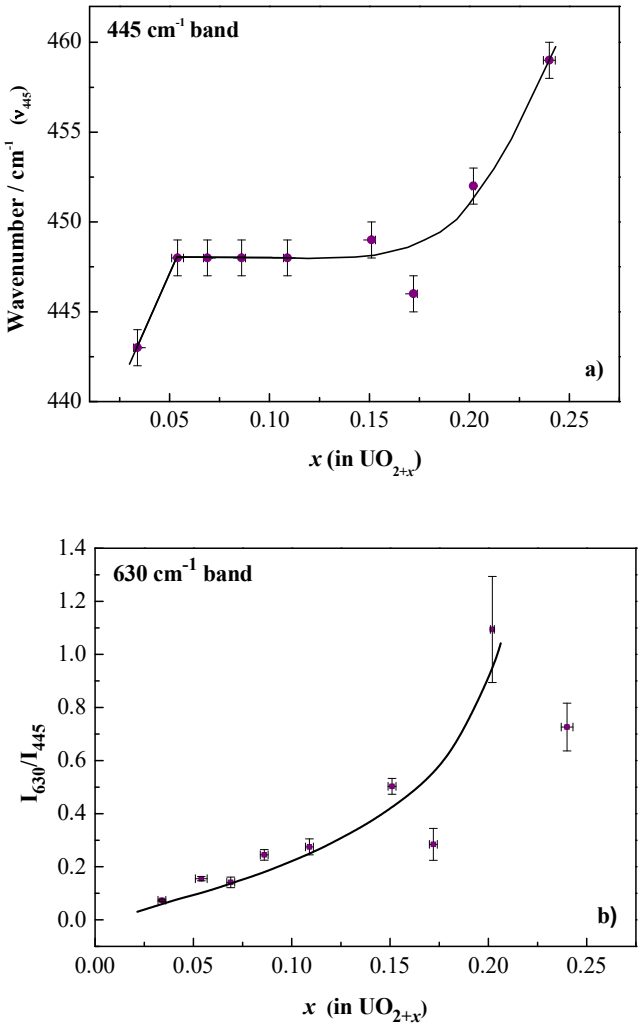

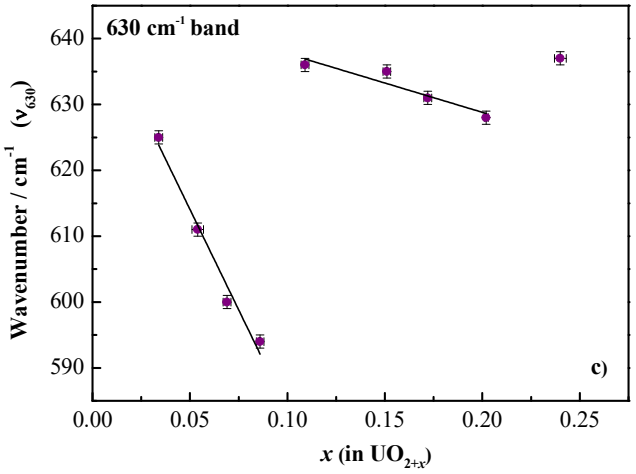

Fig. 6. a) Wavenumber of the 445 cm^{-1} band (ν_{445}), b) normalized maximum intensity, with respect to the 445 cm^{-1} band, of the 630 cm^{-1} band (I_{630}/I_{445}) and c) wavenumber of the 630 cm^{-1} band (ν_{630}), as a function of x (in UO_{2+x}). Lines are guides to the eye.

These results allow us to develop a reliable method to characterize the oxidation degree of any UO_{2+x} sample for $x < 0.20$ using Raman spectroscopy. Since the wavenumber of the 630 cm^{-1} band (v_{630}) shows two well defined and differentiated trends before and after $UO_{2.09}$-$UO_{2.11}$ (Fig. 6c), Equations 3 and 4 can be applied in different ranges of the I_{630}/I_{445} ratio (Fig. 6b), which is directly related to x.

$$v_{630} = 645 \pm 4 - (610 \pm 60)\, x, \quad (I_{630}/I_{445} < 0.24) \qquad \text{(Eq. 3)}$$

$$v_{630} = 647 \pm 4 - (90 \pm 20)\, x, \quad (0.27 < I_{630}/I_{445} < 1.09) \qquad \text{(Eq. 4)}$$

Considering now the outcomes of the Raman spectroscopy characterization, the same structure transitions as from XRD results can be detected around $x = 0.11$ and $x = 0.20$. These are remarkably noticed in the wavenumber evolution of the 630 cm^{-1} band, where clear discontinuities are found around these values of x (Fig. 6c), revealing relevant changes in the anion sublattice. The transition at $x = 0.11$ can also be observed in the wavenumber evolution of the 445 cm^{-1} (T_{2g}) band, which shows an upshift at higher

compositions (Fig. 6a). The T_{2g} band is assigned to the U-O fundamental stretching vibration, so an upshift implies a gradual increase in the bond-strength for $x > 0.11$, what might be explained by a higher amount of surrounding oxygen atoms that produce U-O bond compression, thus confirming the idea that oxidation degree and pressure are related quantities.[41] On the other hand, the transition found at $x = 0.20$ is marked by vanishing of the 2LO band (Fig. 4), commonly associated with a cation sublattice distortion.[6] Interestingly, an additional transition around $x = 0.05$, not identified in the XRD analysis, is suggested from the analysis of the shift of the T_{2g} band (Fig. 6a). This band considerably upshifts from $UO_{2.03}$ to $UO_{2.05}$ very likely caused by a higher amount of surrounding oxygens when the composition $UO_{2.05}$ is reached.

Structural evolution in UO_{2+x}

Taking into account the transitions detected both by XRD and Raman analyses, four main regions with distinct behaviors within the UO_{2+x} range have been identified: $x < 0.05$, $0.05 < x < 0.11$, $0.11 < x < 0.20$ and $0.20 < x < 0.25$. On this basis, the following structural evolution may be presumed:

i) $\underline{0 < x < 0.05}$. As soon as quasi-stoichiometric UO_2 oxidation begins, the lattice starts to contract (marked upshift of the T_{2g} Raman band and a_0 lattice constant decrease). This behavior should be due to the progressive incorporation of oxygen atoms within interstitial sites.[4] He and Shoesmith identified the same region by analyzing the small drop in intensity of the 2LO band and the slight increase in intensity of the 630 cm^{-1} band.[6] In this study we have observed a continuous decrease in intensity of the 2LO band and a continuous increase in intensity of the 630 cm^{-1} band around $UO_{2.05}$, with no detectable change in our band analysis.

ii) $0.05 < x < 0.11$. In this region, as extensively assumed, a_0 decreases following a Vegard's law-like behavior. This can be interpreted as follows: at some point around $UO_{2.05}$, the concentration of interstitial oxygen is so high that oxygens start to rearrange themselves in an ordered manner to accommodate the additional oxygens entering the lattice, what yields a gradual lattice contraction due to the formation of new ordered defect structures: the so-called Willis clusters.[5] On the other hand, since the T_{2g} band wavenumber remains almost constant within this x range, the sublattice contraction is not significant, and some kind of structure rearrangement takes place, what would corroborate the Willis clusters' assumption.

iii) $0.11 < x < 0.20$. The T_{2g} band gradually upshifts throughout this region, reflecting a continuous increase in the U-O bond-strength, what can be attributed to a higher and closer amount of surrounding oxygen atoms as oxidation proceeds. Hence the following structure evolution, assumed by He and Shoesmith over the $0.15 \leq x \leq 0.23$ range,[6] can be taken into consideration: at around $UO_{2.11}$, part of the Willis defect structures start to develop to more densely packed regular distributions (cuboctahedral clusters) in order to allow further oxygen incorporation. This should involve a global gradual lattice expansion, as reflected by the increase in the a_0 lattice constant observed in this study. In addition, the appearance of a new peak in the X-ray pattern at $UO_{2.11}$ confirms the latter assumption of an incipient formation of cuboctahedral clusters.

iv) $0.20 < x < 0.25$. Between $UO_{2.20}$ and $UO_{2.25}$, a_0 recovers the Vegard's law-like behavior and the T_{2g} band continues upshifting, what indicates lattice contraction is again taking place. In addition, the disappearance of the 2LO band around $UO_{2.20}$ suggests distortion of the cation sublattice, which remained undisturbed at lower oxidation degrees, and the possible formation of the U_4O_{9-y} phase, since it has been

previously associated with the 0.17-0.22 < x < 0.25 region.[15,16,17,33] This suggests that, when $UO_{2.20}$ is reached, the complete rearrangement of the oxygen atoms in cuboctahedral clusters leads to a new fully ordered superstructure containing oxygen vacancies (U_4O_{9-y}), which are progressively filled in, thus inducing once again a continuous contraction of the lattice.

4. CONCLUSIONS

A systematic Raman and XRD study of UO_{2+x} powder oxides with controlled degree of non-stoichiometry from x = 0.03 to x = 0.24 has been for the first time presented.

X-ray diffraction detailed analysis shows that the commonly assumed Vegard's law-like behavior is not applicable to the whole hyperstoichiometric UO_{2+x} range. Three different equations are required to describe the lattice constant evolution over such range and precludes using XRD results to calculate x. However, we have found that Raman spectroscopy can be used for this purpose after the analysis of the 630 cm^{-1} Raman band and we have proposed a method to characterize the oxidation degree of any UO_{2+x} oxide (for x < 0.20).

The simultaneous analysis of the Raman and XRD results has allowed us to identify three structural transitions around x = 0.05, 0.11 and 0.20, and to provide an explanation of the structural evolution within the cubic lattice, as follows: i) up to $UO_{2.05}$, a progressive incorporation of oxygen atoms within interstitial sites occurs; ii) between $UO_{2.05}$ and $UO_{2.11}$, these point defects start to rearrange themselves in ordered defect structures or Willis clusters; iii) around $UO_{2.11}$, part of the Willis clusters start to develop into more densely packed cuboctahedral clusters; iv) finally, a complete rearrangement of the oxygen atoms in cuboctahedral clusters at around $UO_{2.20}$ leads to a

new fully ordered superstructure containing oxygen vacancies (U_4O_{9-y}), which are gradually filled in up to at least $UO_{2.24}$.

5. ACKNOWLEDGMENTS

This work was supported by ENRESA within the project Nº 079000189, entitled "Aplicación de técnicas de caracterización en el estudio de la estabilidad del combustible nuclear irradiado en condiciones de almacenamiento" (ACESCO).

6. REFERENCES

[1] R. J. McEachern and P. Taylor, *J. Nucl. Mater.*, 1998, **254**, 87-121.

[2] C. Ferry, C. Poinssot, C. Cappelaere, L. Desgranges, C. Jégou, F. Miserque, J. P. Piron, D. Roudil and J. M. Gras, *J. Nucl. Mater.*, 2006, **352**, 246-253.

[3] B. T. M. Willis, *Proc. Br. Ceram. Soc.,* 1964, **1**, 9-19.

[4] B. T. M. Willis, *Nature,* 1963, **197**, 755-756.

[5] B. T. M. Willis, *Acta Cryst.,* 1978, **A34**, 88-90.

[6] H. He and D. Shoesmith, *Phys. Chem. Chem. Phys.*, 2010, **12**, 8108-8117.

[7] H. Hering and P. Pério, *Bull Soc. Quim.*, 1952, **M. 531**.

[8] L. Desgranges, G. Baldinozzi, P. Simon, G. Guimbretière and A. Canizares, *J. Raman Spectrosc.*, 2012, **43**, 455-458.

[9] P. Jolibois, *C. R. Acad. Sci.,* 1947, **224**, 1395-1396.

[10] L. Desgranges, G. Baldinozzi, G. Rousseau, J. C. Nièpce and G. Calvarin, *Inorg. Chem.*, 2009, **48**, 7585-7592.

[11] G. Rousseau, L. Desgranges, F. Charlot, N. Millot, J.C. Nièpce, M. Pijolat, F. Valdivieso, G. Baldinozzi and J. F. Berar, *J. Nucl. Mater.*, 2006, **355**, 10-20.

[12] L. Quémard, L. Desgranges, V. Bouineau, M. Pijolat, G. Baldinozzi, N. Millot, J. C. Nièpce and A. Poulesquen, *J. Eur. Ceram. Soc.*, 2009, **29**, 2791-2798.

[13] F. Grønvold and H. Haraldsen, *Nature*, 1948, **162,** 69-70.

[14] F. Grønvold, *J. Inorg. Nucl. Chem.*, 1955, **1,** 357-370.

[15] L. Lynds, W. A. Young, J. S. Mohl and G. G. Libowitz, *Adv. Chem.*, 1962, **39**, 58-65.

[16] T. Ishii, K. Naito and K. Oshima, *Solid State Commun.*, 1970, **8**, 677-683.

[17] T. Matsui and K. Naito, *J. Nucl. Mater.*, 1975, **56**, 327-335.

[18] V. A. Alekseyev, L. A. Anan'yeva and R. P. Rafal'skiy, *Int. Geol. Rev.*, 1981, **23**, 1229-1236.

[19] R. E. Rundle, N. C. Baenziger, A. S. Wilson and R. A. McDonald, *J. Am. Chem. Soc.*, 1948, **70**, 99-105.

[20] G. C. Allen, I. S. Butler and N. A. Tuan, *J. Nucl. Mater.*, 1987, **144**, 17-19.

[21] M. L. Palacios and S. H. Taylor, *Appl. Spectrosc.*, 2000, **54**, 1372-1378.

[22] E. A. Stefaniak, A. Alsecz, I. E. Sajó, A. Worobiec, Z. Máthé, S. Török and R. Van Grieken, *J. Nucl. Mater.*, 2008, **381**, 278-283.

[23] F. Pointurier and O. Marie, *Spectrochim. Acta, Part B*, 2010, **65**, 797-804.

[24] D. Manara and B. Renker, *J. Nucl. Mater.*, 2003, **321**, 233-237.

[25] L. Jun-bo, L. Gan and G. Shu-lan, *Spectrosc. Spect. Anal.*, 2014, **34 (2)**, 405-409.

[26] S. Aronson, R. B. Roof and J. Belle, *J. Chem. Phys.*, 1957, **27**, 137-144.

[27] R. Fritsche, Sussieck-Fornefeld C. Min.-Petr. Inst., Univ. Heidelberg, Germany, ICDD Grant-in-Aid, 1988.

[28] P. A. Tempest, P. M. Tucker and J. W. Tyler, *J. Nucl. Mater.*, 1988, **151**, 251-268.

[29] P. Taylor, E. A. Burgess and G. G. Owens, *J. Nucl. Mater.*, 1980, **88**, 153-160.

[30] R. E. Einziger, L. E. Thomas, H. C. Buchanan and R. B. Stout, *J. Nucl. Mater.*, 1992, **190**, 53-60.

[31] K. Naito, T. Ishii, Y. Hamaguchi and K. Oshima, *Solid State Commun.*, 1967, **5**, 349-352.

[32] L. Nowicki, F. Garrido, A. Turos and L. Thomé, *J. Phys. Chem. Solids*, 2000, **61**, 1789-1804.

[33] B. E. Schaner, *J. Nucl. Mater.*, 1960, **2**, 110-120.

[34] B. Belbeoch, J. C. Boivineau and P. Pério, *J. Phys. Chem. Solids*, 1967, **28**, 1267-1275.

[35] C. F. Miller, U. Merten and J. T. Porter, *Chemistry of uranium-oxygen systems: Final report*, U.S. Atomic Energy Commission, Division of Technical Information, San Diego, California, 1961.

[36] P. R. Graves, *Appl. Spectrosc.*, 1990, **144**, 1665-1667.

[37] P. G. Marlow, J. P. Russell and J. R. Hardy, *Philos. Mag.*, 1966, **14**, 409-410.

[38] T. Livneh and E. Sterer, *Phys. Rev. B*, 2006, **73**, 085118-085119.

[39] J. Shoenes, *J. Chem. Soc., Faraday Trans. 2*, 1987, **83**, 1205-1213.

[40] G. Guimbretière, L. Desgranges, A. Canizares, G. Carlot, R. Caraballo, C. Jégou, F. Duval, N. Raimboux, M. R. Ammar and P. Simon, *Appl. Phys. Lett.*, 2012, **100**, 251914.

[41] A. Vegas, J. Mejía-López, A. H. Romero, M. Kiwi, D. Santamaría-Pérez and V. G. Baonza, *Solid State Sci.*, 2004, **6**, 809–814.